

## Anisotropic Cooperative Structural Rearrangements in Sheared Supercooled Liquids

Akira Furukawa,<sup>1</sup> Kang Kim,<sup>2</sup> Shinji Saito,<sup>2</sup> and Hajime Tanaka<sup>1</sup>

<sup>1</sup>*Institute of Industrial Science, University of Tokyo, Meguro-ku, Tokyo 153-8505, Japan*

<sup>2</sup>*Institute for Molecular Science, Nishigonaka, Okazaki 444-8585, Japan*

(Received 4 August 2008; published 9 January 2009)

A supercooled liquid generally exhibits marked shear-thinning behavior, but its detailed mechanism remains elusive. Here we study the dynamics of structural rearrangements in supercooled liquids under shear, using two-dimensional (2D) molecular dynamics simulation. To elucidate the relationship between heterogeneous dynamics and the rheological behavior, we extend the *four-point* correlation function, which has been used for analyzing “dynamic heterogeneity” in a quiescent condition, to a system under steady shear. In the Newtonian regime, the rearrangement dynamics is strongly heterogeneous in space, but remains isotropic. Contrary to this, in the non-Newtonian regime, where marked shear-thinning behavior appears, we find a novel dynamic effect: The mobile region tends to form anisotropic “*fluidized bands*.” This finding suggests a link between nonlinear rheology and inhomogenization of flow.

DOI: 10.1103/PhysRevLett.102.016001

PACS numbers: 83.10.Mj, 47.50.-d, 61.25.-f, 83.80.Ab

Nonequilibrium dynamics of supercooled liquids and glasses [1,2], particularly, glassy dynamics under shear [3], has been extensively investigated from both fundamental and applications viewpoints. As observed in many complex fluids such as polymer solutions and colloidal suspensions [4], marked shear-thinning behavior is also seen in a glass-forming liquid. In numerical simulations of supercooled liquids [5–9], the shear viscosity  $\eta$  and the  $\alpha$ -relaxation time  $\tau_\alpha$  are found to decrease with increasing the shear rate  $\dot{\gamma}$  as  $\eta \propto \tau_\alpha \sim \dot{\gamma}^{-\nu}$  with  $\nu \lesssim 1$ . One of the most intriguing findings is that despite such a distinct shear-thinning behavior, the structure and its relaxation dynamics captured via the two-body correlation function hardly show any anisotropy [5,6], which was also supported by theoretical analysis based on mode coupling theory (MCT) [6,10,11] and experiments [12]. This makes a marked contrast to usual complex fluids, in which non-Newtonian behavior is associated with shear-induced anisotropy or structural change [4,13,14]. The origin of this difference is not at all clear. There are two possibilities: (i) There is an intrinsic difference in the origin of the nonlinear rheology between glass-forming liquids and complex fluids; (ii) something is amiss in the above argument. Here we aim at answering this fundamental question.

The static structure factor of a glass-forming liquid exhibits little change across the glass transition, which apparently suggests the absence of a mesoscopic structure (or order) coupled with shear and thus seems to support the above possibility (i). However, the existence of “dynamic heterogeneity” has recently been established by experiments [15,16] and simulations [5,17–20]: In a supercooled liquid, some regions temporally contain more mobile particles, whereas the other regions contain more immobile particles. It was reported that there exist dynamically correlated structures [5,18,19,21]. Natural questions to be raised are “does such a correlated structure associated with dynamic heterogeneity become anisotropic under shear

flow?” and, then, “is it responsible for non-Newtonian behavior?” A previous simulation study [5] showed that a snapshot of such dynamically correlated structures under steady shear flow does not exhibit any obvious anisotropy; however, there is a possibility that shear-induced structures are washed out by thermal fluctuations even if they exist. Recent experiments [12,22] showed the existence of a large scale “fluidized” band or a conspicuous nonaffine shear deformation flow for glasses under shear. Although these experiments were made for glasses and not for supercooled liquids, similar behavior may be observed in sheared supercooled liquids. To seek such a possibility, here we systematically reinvestigate the structural rearrangement dynamics in sheared supercooled liquids, focusing on how dynamic heterogeneity responds to shear flow.

We used a 2D model liquid, which is a mixture of two atomic species,  $A$  and  $B$  with  $N_A = N_B = 10^4$ . The particles interact via a soft-core potential  $v_{ij}(r) = \epsilon(\sigma_{ij}/r)^{12}$  with  $\sigma_{ij} = (\sigma_i + \sigma_j)/2$ , where  $r$  is the distance between two particles,  $\sigma_i$  is the particle size, and  $i, j = A, B$ . The interaction was truncated at  $r = 4.5\sigma_A$ . The mass and size ratios are  $m_B/m_A = 2$  and  $\sigma_B/\sigma_A = 1.4$ , respectively. We fixed the particle number density at a value of  $\rho = (N_A + N_B)/V = 0.8/\sigma_A^2$ , where  $V$  is the system volume ( $V = L^2$ ;  $L = 158.1\sigma_A$ ). Space and time were scaled by  $\sigma_A$  and  $\tau_0 = (m_A\sigma_A^2/\epsilon)^{1/2}$ . We performed the time integration of the SLLOD equations of motion using the Lee-Edwards boundary condition, and the temperature of the system was maintained by the Gaussian constraint thermostat. Here we set the  $x$  axis along the flow direction and the  $y$  axis along the velocity gradient direction. Under homogeneous shear the mean velocity profile is given by  $\langle \mathbf{v} \rangle = \dot{\gamma}y\hat{x}$ , where  $\hat{x}$  is the unit vector along the  $x$  axis [23].

In this Letter, dynamic heterogeneity and the associated correlated dynamics are quantified by extending the four-point correlation function introduced in [20] to a system under steady shear flow: A time-dependent “order param-

ter” is given by  $Q(t) = \int d\mathbf{r}_1 d\mathbf{r}_2 \rho(\mathbf{r}_1, 0) \rho(\mathbf{r}_2, t) w_{12}$ , where  $\rho(\mathbf{r}, t) = \sum_{i=1}^N \delta(\mathbf{r} - \mathbf{r}_i(t))$  is the density. A position  $\mathbf{r}_1 = (x_1, y_1)$  on the reference frame at  $t = 0$  moves to  $\mathbf{r}_1 + \dot{\gamma} t y_1 \hat{\mathbf{x}}$  at a time  $t$  by the mean shear flow, and so the “overlap” function under steady shear flow should be defined as  $w_{12} = w(|\mathbf{r}_2 - \mathbf{r}_1 - \dot{\gamma} t y_1 \hat{\mathbf{x}}|)$ , where  $w(|\mathbf{r}|) = 1$  (0) for  $|\mathbf{r}| < 0.3$  ( $> 0.3$ ). The mean square variance of the order parameter measures the degree of the cooperativity of structural relaxation:  $\chi_4(t) = (\epsilon V / k_B T N^2) [\langle Q^2(t) \rangle - \langle Q(t) \rangle^2]$ . It can be written in the form of spatial integration as  $\chi_4(t) = (\epsilon V / k_B T N^2) \int d\mathbf{r} \tilde{G}_4(\mathbf{r}, t)$ , where  $\tilde{G}_4(\mathbf{r}, t) = \sum_{i,j,k,l} \langle \delta(\mathbf{r} + \mathbf{r}_i(0) - \mathbf{r}_k(0)) w_{ij} w_{kl} \rangle - \langle Q(t) \rangle^2$ . Its Fourier transformation yields the following structure factor  $S_4(\mathbf{k}, t) = (\epsilon / k_B T N \rho) \langle \tilde{\rho}(\mathbf{k}, t) \tilde{\rho}(-\mathbf{k}, t) \rangle$ , where  $\tilde{\rho}(\mathbf{k}, t) = 1/N \sum_{i,j} \delta e^{i\mathbf{k} \cdot \mathbf{r}_i(0)} w_{ij}$ .  $\tilde{G}_4(\mathbf{r}, t)$  [or  $S_4(\mathbf{k}, t)$ ] itself does not exhibit any anisotropy unless the deviatoric motion becomes anisotropic.

Figure 1(a) shows the intermediate scattering function (self-part) for A particles,  $F_s(\mathbf{k}_0, t) = 1/N_A \sum_{i=1}^{N_A} \langle e^{-i[(\mathbf{k}_0 - \dot{\gamma} t \mathbf{k}_{0y} \hat{y}) \cdot \mathbf{r}_i(t) - \mathbf{k}_0 \cdot \mathbf{r}_i(0)]} \rangle$ , where  $|\mathbf{k}_0| = 2\pi$ . As was already shown in [5,6], we can hardly see any angular dependence in  $F_s(\mathbf{k}_0, t)$  even under shear flow. This means that the relaxation dynamics is almost isotropic at least in the two-body correlation function. We define the  $\alpha$ -relaxation time  $\tau_\alpha(\dot{\gamma})$  as  $F_s(\mathbf{k}_0, \tau_\alpha(\dot{\gamma})) \equiv e^{-1}$ . In Figs. 1(c) and 1(d), we show the order parameter  $\langle Q(t)/N \rangle$  and its mean square variance  $\chi_4(t)$ , respectively. With increasing  $\dot{\gamma}$  both the dynamic scattering function and the order parameter decay faster, and the peak of  $\chi_4(t)$  at  $t = \tau_\chi(\dot{\gamma})$  becomes lower. Note that although  $\tau_\chi(\dot{\gamma})$  and  $\tau_\alpha(\dot{\gamma})$  are not so different in our simulation study, the decrease in  $\dot{\gamma}$  leads to a slight increase in  $\tau_\chi(\dot{\gamma})/\tau_\alpha(\dot{\gamma})$ . We also plot the sample-averaged shear stress  $\langle \sigma_{xy}(t) \rangle = 1/2 \sum_{i=1}^N \times \sum_{i \neq j} \langle (\partial v_{ij} / \partial x_i) y_{ij} \rangle$  in Fig. 1(b) for several shear rates. It is worth mentioning that  $\langle \sigma_{xy}(t) \rangle$  exhibits overshoot behavior at  $t \sim \tau_\chi(\dot{\gamma})$ , instead of at  $t \sim \tau_\chi(\dot{\gamma} = 0)$  [5].

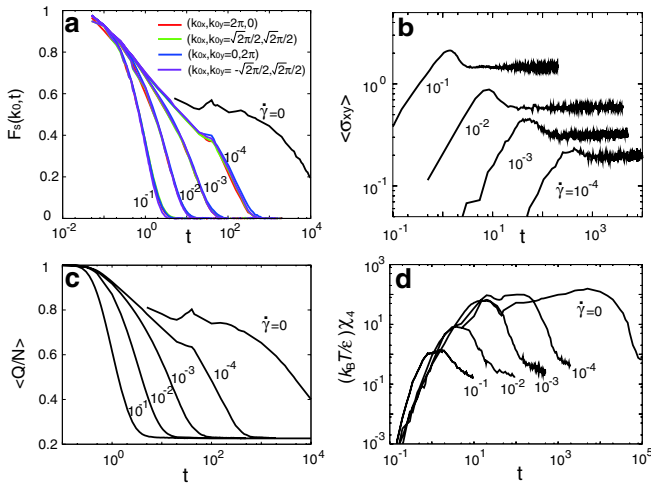


FIG. 1 (color online). (a)  $F_s(\mathbf{k}_0, t)$ , (b)  $\langle \sigma_{xy}(t) \rangle$ , (c)  $\langle Q(t)/N \rangle$ , and (d)  $\chi_4(t)$  for several shear rates at  $k_B T / \epsilon = 0.526$ .

The observed isotropy of  $F_s(\mathbf{k}_0, t)$  has been regarded as supporting evidence for the validity of the concept of the “effective temperature” [7]: A sheared supercooled liquid can be effectively mapped onto the high temperature state without shear flow. Such a concept is attractive since it might open a possibility of the generalized fluctuation-dissipation relation under a nonequilibrium situation. However, we will show below that the dynamic structure of a supercooled liquid becomes strongly anisotropic and heterogeneous under shear.

Figure 2 shows typical snapshots of the deviatoric displacement vector field defined by  $\delta \mathbf{U}(\mathbf{r}_j, \Delta t) \equiv 1/N_j \sum_{i \in V_j} \delta \mathbf{u}_i(\Delta t)$ , where  $\delta \mathbf{u}_i(\Delta t) = [\mathbf{r}_i(t + \Delta t) - \mathbf{r}_i(t) - \dot{\gamma} \Delta t y_i(t) \hat{\mathbf{x}}]$ , and the summation is taken over particles whose center of masses belong to a square area element  $V_j$  (linear size:  $1.76\sigma_A$ ) located at  $\mathbf{r}_j$ . Here  $N_j$  is the number of particles belonging to  $V_j$ . At  $\dot{\gamma} = 0$ , a mobile region is heterogeneously localized and the displacement vector is randomly oriented. On the contrary, under shear flow, several interesting dynamical effects can be seen: The dynamics is not only highly heterogeneous, but also anisotropic: a mobile region tends to form a “fluidized band” along either  $x$  or  $y$  direction. The observed anisotropy appears as the cross-shaped pattern in the structure factor of the local deviatoric displacement vector,  $S_u(\mathbf{k}, \Delta t) = \langle \delta \mathbf{u}_k(\Delta t) \cdot \delta \mathbf{u}_{-k}(\Delta t) \rangle / \langle \delta \mathbf{u}^2 \rangle$  [Fig. 2(c)], where  $\delta \mathbf{u}_k(\Delta t) = 1/\sqrt{N} \sum_{i=1}^N \delta \mathbf{u}_i(\Delta t) e^{i\mathbf{k} \cdot \mathbf{r}_i(t)}$ , and  $\langle \delta \mathbf{u}^2 \rangle = 1/N \sum_i \langle \delta \mathbf{u}_i(\Delta t)^2 \rangle$  [24]. The shear stress acting on the system under a simple shear flow is illustrated by the red arrows in Fig. 2(c). As can be seen from this, the  $x$  and  $y$  directions are equivalent for band formation, which leads to the equal frequency of appearance of bands along the two axes. However, if we set solid boundaries at  $y = L/2$  and  $y = -L/2$ , which is an ordinary experimental con-

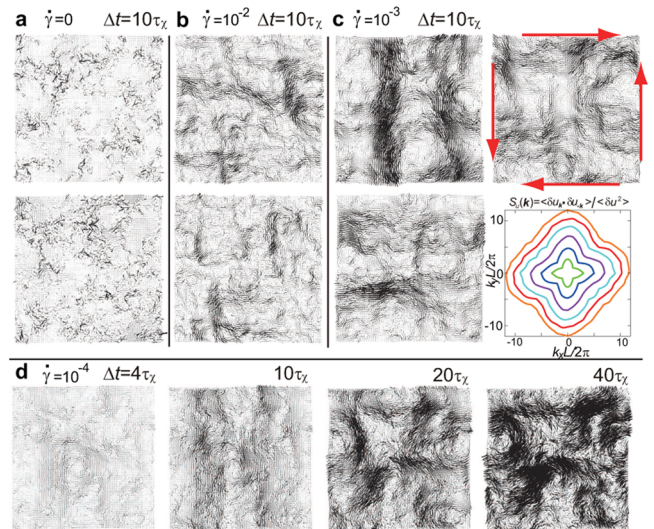


FIG. 2 (color online). Snapshots of  $\delta \mathbf{U}(\mathbf{r}_j, \Delta t)$  for various  $\dot{\gamma}$  at  $k_B T / \epsilon = 0.526$ . Note that another definition,  $\delta \tilde{\mathbf{U}}(\mathbf{r}_j, \Delta t) \equiv 1/N_j \sum_{i \in V_j} [\mathbf{r}_i(\Delta t) - \mathbf{r}_i(0) - \int_0^{\Delta t} dt' \dot{\gamma} y_i(t') \hat{\mathbf{x}}]$ , gives almost the same spatial structure as  $\delta \mathbf{U}(\mathbf{r}_j, \Delta t)$  for the present  $\Delta t$ .

figuration, the growth of fluidized-bands along the  $y$  axis should be suppressed.

The temporal growth of anisotropic bands can be seen in the time evolution of  $S_4(\mathbf{k}, \Delta t)$  at  $\dot{\gamma} = 0.001$  [Fig. 3(a)]. For a shorter time  $t \lesssim \tau_\chi (\sim \tau_\alpha)$ , in which a particle is trapped in its “cage”, random thermal forces overwhelm externally applied forces, resulting in the isotropic pattern of  $S_4(\mathbf{k}, \Delta t)$ . For a longer time  $t \gtrsim \tau_\chi$ , on the other hand, shear-induced cage breaking occurs cooperatively in either  $x$  or  $y$  direction, resulting in the cross-shaped pattern of  $S_4(\mathbf{k}, \Delta t)$  or  $S_u(\mathbf{k}, \Delta t)$ . This suggests a link between the stress overshoot behavior [Fig. 1(b)] and the inhomogenization of flow. The novel four-point correlation analysis developed by Flenner and Szamel revealed correlated directional motion even in the absence of shear flow [25]. Figure 3(a) may be viewed as a dynamic process in which such directional but randomly oriented motion is organized into anisotropic coherent motion under shear. Figure 3(b) shows several particle trajectories for the immobile (left) and the mobile region (right). For a shorter time ( $t \lesssim \tau_\chi$ ), the rattling motion of a particle in its cage is dominant in both mobile and immobile regions. For a longer time ( $t \gtrsim \tau_\chi$ ), on the other hand, we can see distinct directional motion along the  $y$  axis in the fluidized mobile region.

It is worth noting here that the nonaffine nature of deformation increases with decreasing  $\dot{\gamma}$ . For sufficiently small shear rates  $\dot{\gamma} \lesssim 0.001$  ( $k_B T/\epsilon = 0.526$ ) the anisotropic external disturbance becomes so weak that the lifetime of the correlated dynamics becomes long enough for “bands” to extend across the system. Recent experiments on a sheared glass suggest that the localization of a fluidized region becomes more pronounced for a weaker shear rate [12]. This is qualitatively consistent with our result,

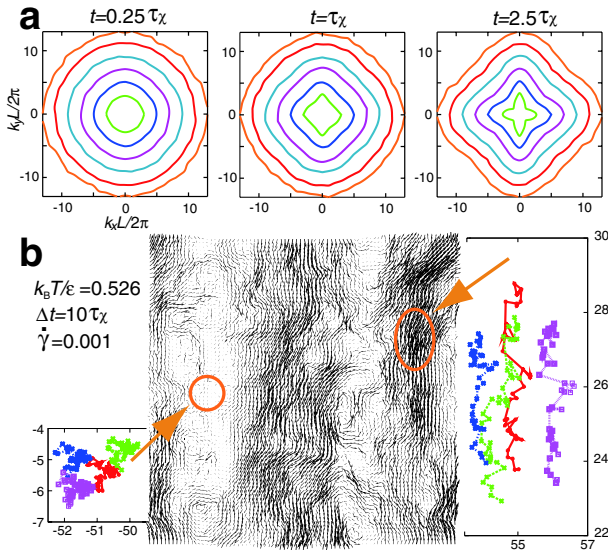


FIG. 3 (color online). (a) Temporal change in  $S_4(\mathbf{k}, \Delta t)$ . (b) A snapshot of  $\delta U(\mathbf{r}_j, \Delta t)$  at  $\dot{\gamma} = 0.001$ . Particle trajectories are also shown in both the less mobile region (left) and the mobile region (right), where a point-to-point interval is about  $0.25\tau_\chi$ .

although the experiments are made for a glass (not a supercooled liquid). We note that fluidized bands are not permanent, but disappear after a certain time, and then reappear: They are spatiotemporally fluctuating. Under steady shear flow, thus, such self-organization and self-collapsing processes are repeated over and over as in turbulence [26].

Now we focus on a link between the above-described anisotropic cooperative dynamics and the non-Newtonian behavior of a supercooled liquid. In Fig. 4, we show the  $\dot{\gamma}$ -dependence of the steady-state shear viscosity  $\eta(\dot{\gamma})$  (a) and the spatial correlation of the displacement field (b). In the linear (Newtonian) regime, rearrangement dynamics is almost isotropic. On the other hand, in the nonlinear (non-Newtonian) regime, where marked shear-thinning behavior ( $\eta \sim \dot{\gamma}^{-0.8}$ ) appears, the anisotropy becomes conspicuous in the cooperative dynamics. We note that the shear-thinning behavior starts at a shear rate much lower than that expected from MCT scenario [6,10,11],  $\dot{\gamma} = 1/\tau_\alpha$  ( $\dot{\gamma} = 0$ ). For  $k_B T/\epsilon = 0.526$ , for example, the shear thinning starts at  $\dot{\gamma}_c \sim 10^{-6}$ , but  $1/\tau_\alpha = 10^{-4} \sim 10^{-3}$ . This suggests that there may be a structural relaxation process much slower than  $\tau_\alpha$  characterizing the decay of the two-body correlation. We speculate that the characteristic time  $1/\dot{\gamma}_c$  may mark the lifetime of long-lived immobile structures, which indeed keep their internal particle configurations for a time much longer than  $\tau_\alpha$  [see Fig. 2(a)]. The origin of such immobile structures, structural order [21] or something else, remains the subject for future study.

Next we investigate the correlation between the “mobility” of particles and the shear stress born by them. In athermal systems a negative correlation between particle mobility and local shear stress can be easily seen even in snapshots of velocity and stress fields (see, e.g., [9,27–29]), whereas in thermal systems such a correlation is almost completely masked by thermal fluctuations [5]. Here we demonstrate that statistical averaging removes thermal fluctuations and thus reveals such a *mobility* dependence.

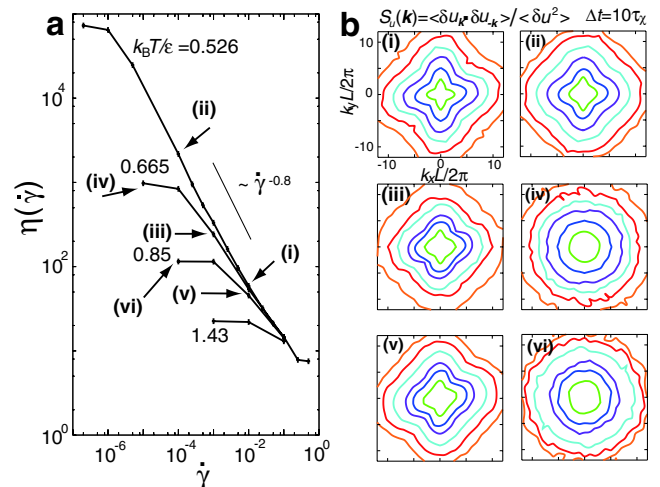


FIG. 4 (color online). (a)  $\eta(\dot{\gamma})$  vs  $\dot{\gamma}$  for various  $k_B T/\epsilon$ 's. (b)  $S_u(\mathbf{k}, \Delta t = 10\tau_\chi)$  for  $(T, \dot{\gamma})$  numbered (i) to (vi) in (a).

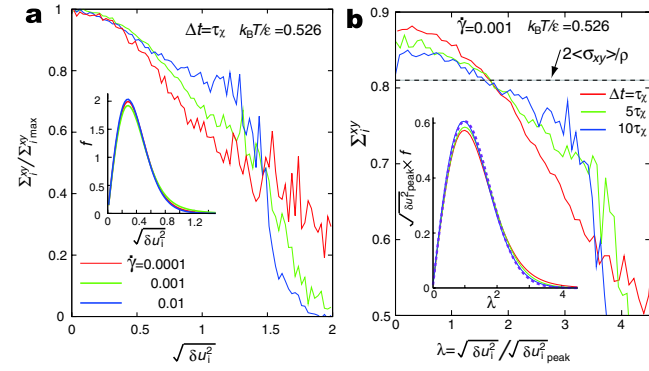


FIG. 5 (color online). (a)  $\Sigma_i^{xy}(\Delta t)$  scaled by its maximum value  $\Sigma_{i \max}^{xy}(\Delta t)$  for three values of  $\dot{\gamma}$  for  $\Delta t \equiv \tau_\chi$ . The inset shows the normalized distribution function of  $\sqrt{\delta u_i^2(\Delta t)}$ , which satisfies  $\int_0^\infty dx f(x) = 1$ . (b)  $\Sigma_i^{xy}(\Delta t)$  is plotted against  $\lambda = \sqrt{\delta u_i^2(\Delta t)} / \sqrt{\delta u_i^2(\Delta t)_{\text{peak}}}$  for three values of  $\Delta t$  at  $\dot{\gamma} = 0.001$ . Here  $\sqrt{\delta u_i^2(\Delta t)_{\text{peak}}}$  is the peak position of the distribution function, which grows as  $\sim \Delta t^{1/2}$ . The inset shows the scaled distribution function  $\sqrt{\delta u_i^2(\Delta t)_{\text{peak}}} f$ , which approaches the Gaussian indicated by the purple dotted curve with increasing  $\Delta t$ , as a function of  $\lambda$ .

The shear stress acting on particle  $i$  at time  $t$  can be obtained as  $\sigma_i^{xy}(t) = \sum_{j \neq i} (\partial v_{ij} / \partial x_i) y_{ij}$ , where  $\mathbf{r}_{ij} = \mathbf{r}_i - \mathbf{r}_j$ . In Fig. 5(a), we plot the shear stress averaged during a time interval  $\Delta t = \tau_\chi$ ,  $\Sigma_i^{xy}(\Delta t) = 1/\Delta t \langle \int_0^{\Delta t} dt \sigma_i^{xy}(t) \rangle$ , as a function of the square root of the deviatoric displacement,  $\sqrt{\delta u_i^2(\Delta t)}$ . We can see that less mobile particles can sustain more shear stress, but for relatively mobile particles ( $\sqrt{\delta u_i^2(\Delta t)} \gtrsim 0.3$ )  $\Sigma_i^{xy}(\Delta t)$  decays gradually. Figure 5(b), on the other hand, shows that  $\Sigma_i^{xy}(\Delta t)$  for different  $\Delta t$ 's. With increasing  $\Delta t$ , the distribution function  $f$  asymptotically approaches a Gaussian and the “mobility” dependence of  $\Sigma_i^{xy}(\Delta t)$  becomes weaker. This is because long-time averaging ( $\Delta t \gg \tau_\chi$ ) makes the mobility of each particle and the resultant  $\Sigma_i^{xy}(\Delta t)$  homogeneous [ $\lim_{\Delta t \rightarrow \infty} \Sigma_i^{xy}(\Delta t) = 2\langle \sigma_{xy} \rangle / \rho$ , the dashed line in Fig. 5(b)].

To sum, contrary to a common belief, we demonstrated that in the nonlinear regime a supercooled liquid under shear exhibits anisotropic cooperative structural rearrangements, which can be seen by the four-point correlator but not by the two-point correlator. Our finding calls for further improvement or modification of the present mean-field picture and the concept of the effective temperature for a sheared glassy liquid, where the shear field is treated as an isotropic perturbation. Finally, according to our preliminary 3D simulations, the basic features of our 2D results are retained in 3D: The particle diffusivity is more enhanced (equally) in the  $x$  (flow) and  $y$  (shear) directions than in the  $z$  (vorticity) direction under shear flow, resulting

in a cross-shaped pattern of  $S_u(\mathbf{k}, \Delta t)$  on the  $k_x - k_y$  plane in the non-Newtonian regime [30].

We wish to thank K. Miyazaki and R. Yamamoto for valuable comments. A. F. and H. T. acknowledge a grant-in-aid from JSPS and MEXT, respectively. Calculations were partially carried out at RCCS, Okazaki, Japan.

- [1] W. Götze and L. Sjögren, Rep. Prog. Phys. **55**, 241 (1992).
- [2] K. Binder and W. Kob, *Glassy Materials and Disordered Solids* (World Scientific, Singapore, 2005).
- [3] *Jamming and Rheology*, edited by A. J. Liu and S. R. Nagel (Taylor and Francis, New York, 2003).
- [4] R. G. Larson, *The Structure and Rheology of Complex Fluids* (Oxford University Press, Oxford, 1999).
- [5] R. Yamamoto and A. Onuki, Phys. Rev. E **58**, 3515 (1998).
- [6] K. Miyazaki *et al.*, Phys. Rev. E **70**, 011501 (2004).
- [7] J.-L. Barrat and L. Berthier, Phys. Rev. E **63**, 012503 (2000); L. Berthier and J.-L. Barrat, J. Chem. Phys. **116**, 6228 (2002).
- [8] L. Angelani *et al.*, Phys. Rev. E **66**, 061505 (2002).
- [9] F. Varnik, J. Chem. Phys. **125**, 164514 (2006).
- [10] K. Miyazaki and D. R. Reichman, Phys. Rev. E **66**, 050501 (R) (2002).
- [11] M. Fuchs and M. E. Cates, Phys. Rev. Lett. **89**, 248304 (2002); Faraday Discuss. **123**, 267 (2003).
- [12] R. Besseling *et al.*, Phys. Rev. Lett. **99**, 028301 (2007).
- [13] A. Onuki, J. Phys. Condens. Matter **9**, 6119 (1997).
- [14] A. Onuki, *Phase Transition Dynamics* (Cambridge University Press, Cambridge, England, 2002).
- [15] H. Sillescu, J. Non-Cryst. Solids **243**, 81 (1999).
- [16] M. D. Ediger, Annu. Rev. Phys. Chem. **51**, 99 (2000).
- [17] M. M. Hurlley and P. Harrowell, Phys. Rev. E **52**, 1694 (1995); D. N. Perera and P. Harrowell, *ibid.* **54**, 1652 (1996).
- [18] R. Yamamoto and A. Onuki, Phys. Rev. Lett. **81**, 4915 (1998).
- [19] C. Donati *et al.*, Phys. Rev. Lett. **80**, 2338 (1998); C. Donati *et al.*, Phys. Rev. E **60**, 3107 (1999).
- [20] N. Lačević *et al.*, J. Chem. Phys. **119**, 7372 (2003).
- [21] H. Shintani and H. Tanaka, Nature Phys. **2**, 200 (2006); T. Kawasaki *et al.*, Phys. Rev. Lett. **99**, 215701 (2007); K. Watanabe and H. Tanaka, *ibid.* **100**, 158002 (2008).
- [22] P. Schall *et al.*, Science **318**, 1895 (2007).
- [23] D. C. Rapaport, *The Art of Molecular Dynamics Simulation* (Cambridge University Press, Cambridge, England, 1995).
- [24] We note that the results reported here are free from the finite size effect, which was confirmed by comparing simulation results for  $N = 4000 (L = 70.7\sigma_A)$ ,  $N = 10000 (L = 111.8\sigma_A)$ , and  $N = 60000 (L = 273.9\sigma_A)$ .
- [25] E. Flenner and G. Szamel, J. Phys. Condens. Matter **19**, 205125 (2007).
- [26] U. Frish, *Turbulence* (Cambridge University Press, Cambridge, England, 1995).
- [27] A. Onuki, Phys. Rev. E **68**, 061502 (2003).
- [28] C. E. Maloney and A. Lemaître, Phys. Rev. E **74**, 016118 (2006).
- [29] A. Tanguy *et al.*, Eur. Phys. J. E **20**, 355 (2006).
- [30] A. Furukawa *et al.* (unpublished).